CIVIL ENGINEERING JOURNAL

Article no. 30

THE CIVIL ENGINEERING JOURNAL 3-2024

DUST DISTRIBUTION PATTERN AND OPTIMIZATION OF TUNNEL VENTILATION SYSTEM

Xuhui Zhang[1, 2], Hanwen Lai[1], Zeren Peng[1], Hengxing Zhong[1], Yashi Liao[1], Lian Lian Tan[3] and Jingping Liao[4, 5]

1. *University of Engineering and Design, Hunan Normal University, Changsha, 410081, China*
2. *University of Mechanical and Electrical Engineering, Central South University, Changsha Hunan 410083, China*
3. *Hunan Lianzhi Technology Co.,Ltd. Changsha Hunan 410219, China*
4. *Beijing Technology Research Branch, CCTEG Tiandi Science & Technology Co., Ltd, Beijing 100013, China*
5. *Intelligent Mining Research Institute, CCTEG Chinese Institute of Coal Science, Beijing 100013, China; woshiliao1989@163.com*

ABSTRACT

This paper focuses on examining the effectiveness of a long-pressure and short-pumping ventilation system in a tunnel construction project. Utilizing computational fluid dynamics theory and ventilation system design principles, the study involves numerical simulations through finite element method to analyze dust distribution within the tunnel. The research investigates the effect of the distance of the duct from the working face and pumping ratio on dust concentration. The results indicate that optimal ventilation and dust removal occur when Lpressure set at 20m, Lpumping set at 3m, and pumping ratio is 0.7, the dust concentration can be reduced to less than 250 mg/m3 within 10m of the tunnel face which ensures the requirement of dust reduction in the main working area of workers and ensure a safer working environment.

KEYWORDS

Tunnel ventilation system, Dust concentration, Long-pressure and short-pumping, Pumping ratio, Duct

INTRODUCTION

The rapid development of underground engineering machinery has led to widespread use of roadheaders across various fields [1]. However, the full-section hard rock roadheader produces significant amounts of dust during tunnel construction, posing risks to workers such as pneumoconiosis and safety hazards [2-3]. Dust accumulation can also interfere with equipment operation. Therefore, the ventilation and dust removal system is crucial to ensure worker safety, equipment functionality, and control of environmental conditions within the tunnel [4-6]. Numerous scholars have conducted research on this issue, proposing innovative solutions. For instance, Ni et al. [7] introduced a pseudo-concentrated particle population model that views dust as a "two-phase

flow" of gas and solid particles, revealing the spatial distribution of particle concentration. Hargreaves et al. [8] employed a kinetic approach to develop tunnel ventilation models, enhancing auxiliary ventilation systems to mitigate hazards.

Scholars have also fine-tuned dust removal system models to optimize dust elimination based on dust characteristics. The studies by Parra et al. [9], Wang et al. [10], Lai et al [11], Hussein et al. [12], Klemens et al. [13], SA et al. [14] and Ashrafi et al. [15] demonstrate various approaches to addressing dust control challenges in tunnel construction, showcasing the importance of efficient ventilation systems and dust management protocols in ensuring worker health and safety.

Several scholars have conducted research on ventilation methods for different terrain conditions. Lee et al. [16] conducted a comparative analysis of the pitch angle of the jet fan in a jet fan ventilation system. Torano et al. [17] ultimately identified the optimal pitch angle for enhancing ventilation efficiency. Liu et al. [18] utilized CFD numerical simulation to investigate the effects of ventilation and dust removal systems on dust dispersion distance and average concentration within the excavation area. Meanwhile, Xie et al. [19] explored 16 distinct ventilation conditions, determining effective dust suppression parameters through numerical simulation and field measurements. Yang et al. [20] proposed a modular airflow diversion system that integrates ventilation and dust removal, analyzing airflow-dust coupling behaviors under various conditions and identifying optimal airflow rate ratios and distances between working faces and airflow outlets. Additionally, Von Glehn et al. [21] analyzed the impact of ventilation systems on the thermal working environment and driving equipment in TBM tunnel boring, devising an optimal ventilation scheme for controlling tunnel temperatures. In a separate study, Xia et al. [22] examined the effects of main vent position, main baffle plate, and exhaust air volume on flow field distribution and dust flow characteristics during open-type TBM tunnel boring. Liu et al. [23] investigated dust control in TBM construction tunnels under varying dust extraction flow rates. Lastly, Li et al [24]. developed a cartridge filter to address dust pollution issues during TBM tunnelling in submarine tunnels, successfully reducing dust concentrations within the tunnels following practical tests.

Existing studies have pointed out the hazards associated with high concentrations of dust generated during tunnel construction, the dispersion patterns of dust under varying working conditions, and effective strategies to mitigate tunnel dust concentration. These findings not only advance the field of tunnel construction and dust control but also lay the groundwork for enhancing the tunnel construction environment and guiding the design of ventilation and dust removal systems. Currently, the absence of standardized design approaches for ventilation and dust removal in specific tunnels poses a challenge. Given the diversity in tunnel structures and working environments, as well as variations in the characteristics and operational conditions of comprehensive excavation faces across regions, a one-size-fits-all solution is unattainable. Furthermore, existing research predominantly focuses on the impact of individual factors on tunnel dust removal efficiency, overlooking the combined effects of multiple factors. Thus, a more comprehensive investigation into ventilation and dust removal system design is warranted in diverse tunnel environments. Through a detailed analysis of dust migration within the ventilation system of a tunnel, as illustrated in Figure 1, this study advocates for the adoption of a long-pressure and short-pumping ventilation system. The combination of pressure and pumping satisfies the air supply needs, while also directing dust particles into the dust removal device for purification. By optimizing the configuration of ventilation and dust

removal ducts, and adjusting the distance between the duct and working face while controlling the pumping air volume, a strong circulating flow field will be formed in front of the working face. This approach aims to enhance the efficiency of dust removal and ventilation while maintaining a safe and stable working environment, which keeps the tunnel dust concentration below 250mg/m3. The insights gained from this study are expected to inform best practices in the construction and operation of tunnels.

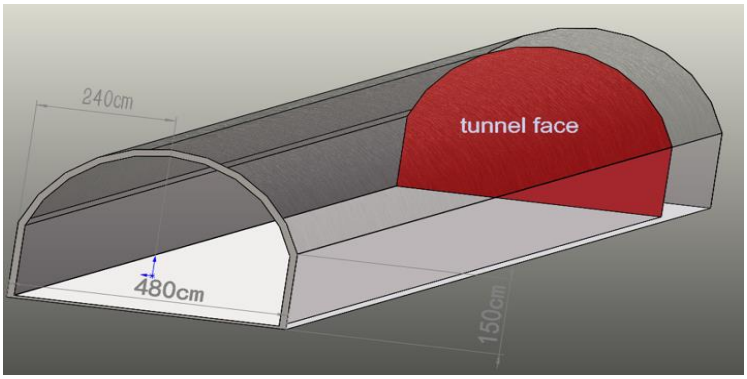

Fig. 1 – Structure of a road tunnel

FINITE ELEMENT MODELLING

Hypothetical condition

In this paper, the physical model of the tunnel is based on several key assumptions. Firstly, it is assumed that the density of air within the tunnel is uniform and that the air itself behaves as an incompressible fluid. Additionally, it is assumed that the air ducts are effectively sealed, with no consideration given to flow and pressure losses within the ducts. Moreover, the wind flow induced by the fan at the inlet or outlet of each property is assumed to remain constant over time, in terms of both pressure and direction. Finally, the flow field within the tunnel is assumed to exhibit steady-state turbulence.

Basic control equations

The law of conservation of mass in a flow field containing incompressible gas, where the gas density is assumed to remain constant over time, can be simplified:

$$\frac{\partial v_x}{\partial_x} + \frac{\partial v_y}{\partial_y} + \frac{\partial v_z}{\partial_z} = 0 \quad (1)$$

Energy in a fluid system:

$$E = i + K + P \quad (2)$$

$$i = cT \quad (3)$$

$$K = \frac{1}{2}(V_x + V_y + V_z) \quad (4)$$

In the formula: *E*: total energy; *i*: internal energy of a fluid system; *c*: specific heat capacity of a fluid; *K*: internal energy of a fluid system; *P*: potential energy of a fluid system; *T*: fluid temperature.

In fluid dynamics, the total energy (*E*) in the system consists of internal energy, kinetic energy,

and potential energy of the fluid. Typically, the focus is on the conservation of internal energy (*i*), with the deduction of kinetic energy (*K)* in the conservation equation. Internal energy (*i*) is directly proportional to the temperature (*T*), leading to the formulation of an energy conservation equation with temperature (*T*) as the variable. The system's energy equation yields insights into the composition and conservation of energy within the fluid in practical fluid problems [25]:

$$\frac{\partial}{\partial_t}(\rho T) + div(\rho \vec{v} T) = div(\frac{k}{c} gradT) + S_T \quad (5)$$

In the formula: *p*: fluid density; *k*: fluid heat transfer coefficient; S_T: viscous dissipative term (in fluid mechanics).

The conservation of momentum law is widely applied, stating that the magnitude of an external force acting on a small fluid element is equal to the rate of change of momentum with time. This law forms the basis for deriving an equation that conserves momentum of the microelement in the x, y, and z directions. This conservation equation can be expressed as follows:

$$\frac{\partial(pu)}{\partial t} + \frac{\partial(puu)}{\partial x} + \frac{\partial(puv)}{\partial y} + \frac{\partial(puw)}{\partial z} = \frac{\partial}{\partial x}\left(\mu \frac{\partial u}{\partial x}\right) + \frac{\partial}{\partial y}\left(\mu \frac{\partial u}{\partial y}\right) + \frac{\partial}{\partial z}\left(\mu \frac{\partial u}{\partial z}\right) - \frac{\partial p}{\partial x} + S_u \quad (6)$$

$$\frac{\partial(pv)}{\partial t} + \frac{\partial(pvu)}{\partial x} + \frac{\partial(pvv)}{\partial y} + \frac{\partial(pvw)}{\partial z} = \frac{\partial}{\partial x}(\mu \frac{\partial v}{\partial x}) + \frac{\partial}{\partial y}(\mu \frac{\partial v}{\partial y}) + \frac{\partial}{\partial z}(\mu \frac{\partial v}{\partial z}) - \frac{\partial p}{\partial y} + S_v \quad (7)$$

$$\frac{\partial(pw)}{\partial t} + \frac{\partial(pwu)}{\partial x} + \frac{\partial(pwv)}{\partial y} + \frac{\partial(pww)}{\partial z} = \frac{\partial}{\partial x}(\mu \frac{\partial w}{\partial x}) + \frac{\partial}{\partial y}(\mu \frac{\partial w}{\partial y}) + \frac{\partial}{\partial z}(\mu \frac{\partial w}{\partial z}) - \frac{\partial p}{\partial z} + S_w \quad (8)$$

In the formula: *μ*: dynamic viscosity coefficient of the fluid, N·s/M^2; *p*: Pressure on the fluid, pa; S_u S_v S_w: Generalised source terms for the dynamical equations in the x, y and z directions.

Geometric modelling of ventilation systems

The simplified tunnel model, as depicted in Figure 2, has a length of 30 m. The tunnel arch has a height of 3.6 m and a width of 4.8 m, resulting in a tunnel section area (A) of 15.15 m^2, with detailed dimensions illustrated in Figure 3. Ventilation and dust removal ducts are suspended on both sides of the tunnel. These ducts are positioned with their axis centers 1.7 m from the vertical center axis and 1.5 m from the ground. Both ducts have a diameter of 0.8 m

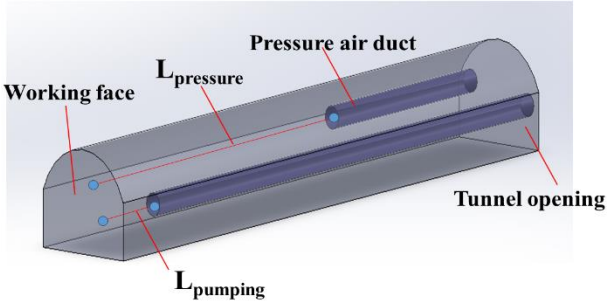

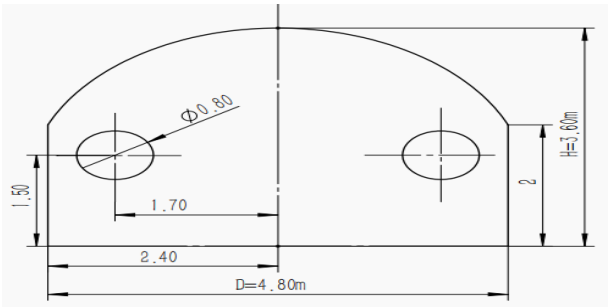

Fig. 2 – Tunnel model sketch *Fig. 3 – Tunnel cross-section dimensions*

When the tunnel section area (A) is 15.15 m^2, the duct distance from the working face can be determined by the empirical formulas working face [30]:

$$L_{pressure} \geq (4\sim5)\sqrt{A}$$

$$L_{pumping} \leq 1.5\sqrt{A} \quad (12)$$

In above formulas, the $L_{pressure}$ denotes the range of 15.56m to 19.45m and the $L_{pumping}$ below 5.84 m.

In this paper, the geometric model of the tunnel includes both the tunnel and air ducts. The mesh division size is set at 0.1m, and the resulting mesh model is depicted in Figure 4.

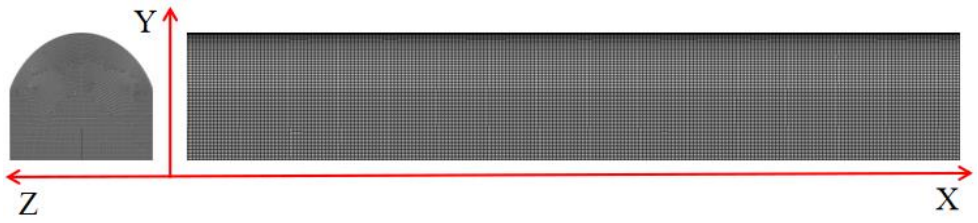

Fig. 4 – Cell mesh diagram of the tunnel

The physical model of the tunnel, as depicted in Figure 5, was established with specific directional indicators: X representing the length direction, Z representing the width direction, and Y representing the height direction. The ZX section of the tunnel model denotes the vertical measurement above the tunnel's ground, set at a height of 1.5m. The XY section corresponds to the center plane of the tunnel's vertical axis, while the ZY section illustrates the tunnel profile at various distances from the tunnel-faced end. Five cross-sections were selected along the negative X-axis direction of the tunnel within the 10m from the working face, specifically at intervals of 1m, 3m, 5m, 7m, and 9m. Subsequently, the Dust Par Mass Concentration (DPM-C) of these five cross-sections was analyzed to conduct data statistics.

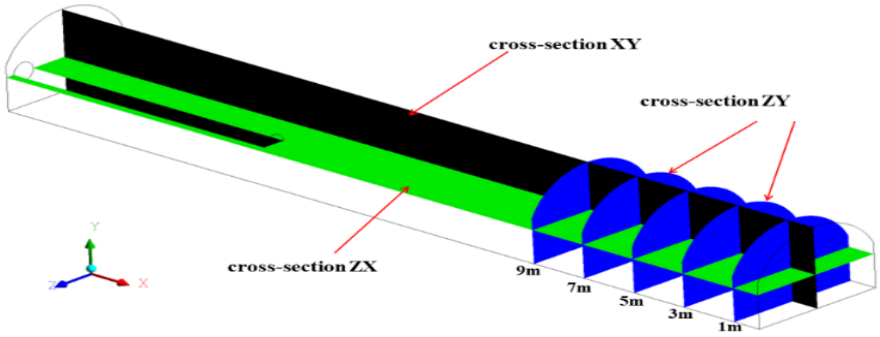

Fig. 5 – Schematic diagram of the physical model of the tunnel

Numerical simulation models

Individual dust particles are used in constructing the Discrete Phase Model (DPM) in an Eulerian-Lagrangian approach [27]. Table 1 shows the specific computational model and Table 2 displays the parameter settings for the Discrete Phase Model.

Tab. 1 - Computational modelling

Calculate Model		Define
Solver		Pressure Based
Space		3D
Time		Steady
Viscous Model		K-epsilon
Energy		Off
Pressure-Velocity Coupling		Coupled
Discrete Phase Model		On
Acceleration of gravity	X	0
	Y	-9.81m/s^2
	Z	0

Tab. 2 – Discrete phase model parameters

Discrete Phase Model	Define
Interaction	Interaction with Continuous Phase
Number of Continuous Phase Iterations per DPM Iteration	10
Max Number of Steps	5000
Length Scale	0.01
Drag Law	Spherical

The tunnel construction ventilation standards specify Q as 600 m^3/min, with duct diameters of 0.8m and a calculated duct cross-sectional area of 0.503 m^2. Per the air volume and velocity conversion formula [28]:

$$V = \frac{Q}{60A} \quad (13)$$

In the formula: *V*: Velocity Air volume Cross-sectional area (m/s); *Q*: Air volume; m^3/min; *A*: Cross-sectional area (m^2).

Setting the specific boundary conditions: Inlet Boundary Type is set to velocity-inlet; Hydraulic Diameter is set to 0.8 m; Outlet Boundary Type is set to Outflow; the DPM Condition of Wall is set to reflect; the Shear Condition is set to no slip and the velocity V_1 at the pressing air volume is calculated to be 19.89 m/s by substituting the air volume and the cross-sectional area of the duct into Equation 1. Similarly, the velocity V_2 at the pumping air volume is determined to be 13.93 m/s.

SIMULATION RESULT ANALYSIS

Effect of the position of pressure duct on dust distribution

The dust concentration distribution in the ZX plane at a height of 1.5m from the ground (the average breathing height of the workers) is intercepted and analyzed. Prior to analysis, distance between the pumping duct and the working face ($L_{pumping}$), with a pumping ratio (r) of 0.7, was set at 3m, and the height distance between the centres of the two ventilation ducts was established at 1.5m. Subsequently, the $L_{pressure}$ was varied at 16m, 18m, 20m, 22m, 24m, and 26m for numerical simulation. The simulation results, shown in Figure 6, provide significant insights into the ventilation system's effectiveness in controlling dust concentration levels.

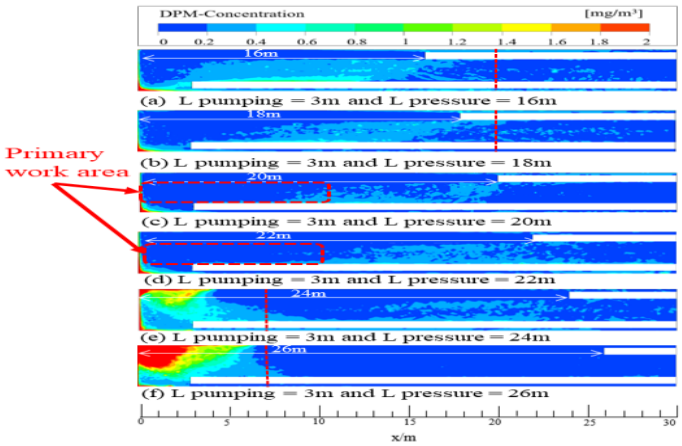

Fig. 6 – Distribution of dust concentration at a height of 1.5m above the ground at different locations of pressure air outlets: (a) $L_{pumping}$ = 3m and $L_{pressure}$ = 16m; (b) $L_{pumping}$ = 3m and $L_{pressure}$ = 18m; (c)$L_{pumping}$ = 3m and $L_{pressure}$ = 20m; (d)$L_{pumping}$ = 3m and $L_{pressure}$ = 22m; (e)$L_{pumping}$ = 3m and $L_{pressure}$ = 24m; (f)$L_{pumping}$ = 3m and $L_{pressure}$ = 26m

As depicted in Figure 6, the distribution of dust accumulation is influenced by the distance of the pressing air outlets to the working face. When the $L_{pressure}$ is in the range of 16m to 18m, denoted in Figure 6(a) and (b), the close distance between the pressing air outlet and the working face results in a significant dispersion of dust beyond the jet area, rendering the pumping duct less effective in controlling the dust concentration. Consequently, the secondary dust spreading distance extends up to about 20m, covering a substantial area of the construction site with higher dust concentrations near the pumping duct compared to the pressing duct. Moreover, as the $L_{pressure}$ is in the range of 20m to 22m, denoted in Figure 6(c) and (d), a well-balanced airflow pattern is achieved with a moderate distance between the pressing air inlet and the working face, facilitating efficient dust flow towards the suction air inlet and restricting dust dispersion to within a 5m. The concentration of dust is primarily confined to the main construction area, emphasizing the effectiveness of ventilation and dust removal in this scenario. However, when the $L_{pressure}$ extends to 24m or 26m, as shown in Figure 6(e) and (f), dust predominantly locates approximately 10m from the working face, leading to high dust concentrations. It can be explained that the large $L_{pressure}$ will diminish wind speed and restrict effective dust discharge, resulting in dust retention near the working face. Consequently, the tunnels experience suboptimal ventilation and dust removal efficacy under these large $L_{pressure}$.

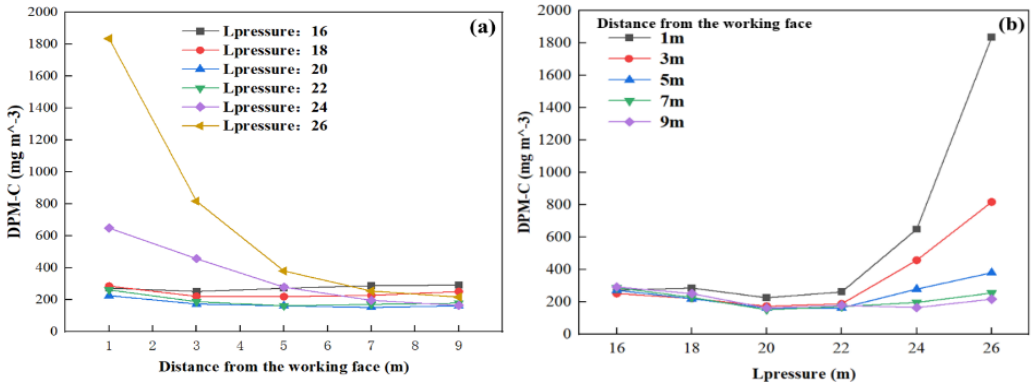

Fig. 7 – Comparison of along-track distribution of dust concentration at different locations of the pressure air outlets: (a) different locations of the pressure air outlet; (b) different distances from the working face.

Upon examining Figure 7(a), it is evident that different $L_{pressure}$ yield varying dust concentrations within the vicinity of the working face. For instance, when the $L_{pressure}$ ranges from 24 to 26m, within 5m from the working face (0<X<5m), the dust concentration experiences a sharp decrease as the distance from working face increases, yet the DPM-C remains above 600 mg/m^3, designating this region as critical for dust control measures. Conversely, with an $L_{pressure}$ between 16 and 18m, at a distance of 5-10m from the working face (3<X<10m), the dust disperses rearward as the distance from working face increases, leading to a gradual increase in concentration, eventually reaching 300 mg/m^3 on average. Subsequently, an $L_{pressure}$ of 20 to 22m results in a diminishing dust mass concentration within a 10m from the working face compared with the $L_{pressure}$ equals 24 and 26m, with the DPM-C being effectively lowered to 250mg/m^3. Notably, the optimum reduction in the DPM-C to 250 mg/m^3 and enhanced dust removal efficiency are achieved at an $L_{pressure}$ of 20m. This outcome not only benefits construction personnel by providing a conducive environment for construction operations but also enhances the overall effectiveness of dust control measures.

Effect of the position of pumping duct on dust distribution

To investigate the effect of the pumping duct position on dust distribution, the $L_{pressure}$ is set at 20m, with a pumping ratio of 0.7 and the height of the center position of the two ventilation ducts at 1.5m. The $L_{pumping}$ is selected as a variable with value of 1m, 2m, 3m, 4m, 5m, and 6m. Figure 8 presents the simulation results under different $L_{pumping}$.

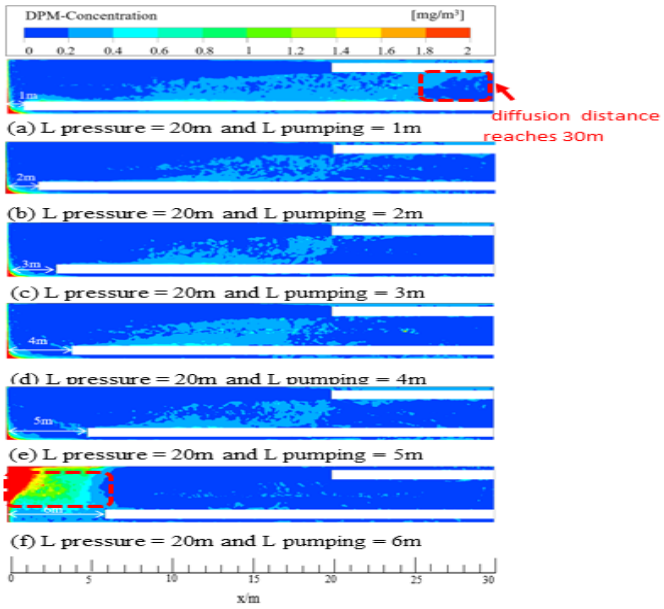

Fig. 8 – Distribution of dust concentration at a height of 1.5m above the ground at different locations of the air pumping outlets: (a) $L_{pressure}$ = 20m and $L_{pumping}$ = 1m; (b) $L_{pressure}$ = 20m and $L_{pumping}$ = 2m; (c) $L_{pressure}$ = 20m and $L_{pumping}$ = 3m; (d) $L_{pressure}$ = 20m and $L_{pumping}$ = 4m; (e) $L_{pressure}$ = 20m and $L_{pumping}$ = 5m; (f) $L_{pressure}$ = 20m and $L_{pumping}$ = 6m

When the position of the air pressure outlet is fixed, the distance of the air pumping outlet from the face has a significant impact on the spread of dust. For instance, at a distance of 1m ($L_{pumping}$ = 1m) as depicted in Figure 8(a), the proximity of the air pumping port to the working face results in the dust being influenced by the impact airflow from the rock breaking activity at the head of the roadheader. Consequently, the dust is driven outward, with some particles escaping the airflow control mechanism of the air pumping system, leading to diffusion into other areas of the tunnel up to a distance of 30m. In contrast, at distances of 2-5m ($L_{pumping}$ = 2~5m) as illustrated in Figure 8(b), (c), (d), (e), the location of the air pumping duct in relation to the working face creates a moderate airflow field that effectively controls the dust generated at the working face. The airflow limits the diffusion distance of the dust within the tunnel, resulting in a relatively reduced coverage area and improving the overall ventilation and dust removal efficiency at the operating face. Conversely, when the distance is 6m ($L_{pumping}$ = 6m) as shown in Figure 8(f), the air pumping duct is too distant from the working face, leading to the airflow being insufficient to drive the dust towards the pumping point effectively. Consequently, a significant accumulation of dust occurs within a 5m from the working face, resulting in high dust concentrations and poor ventilation and dust removal efficacy in that area.

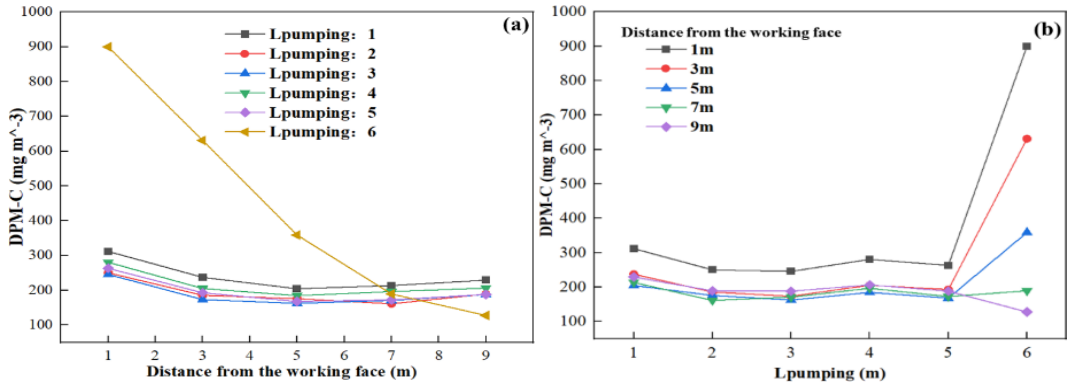

Fig. 9 – Comparison of along-track distribution of dust concentration at different pumping positions: (a) different pumping positions; (b) different distances from the working face.

After analyzing Figure 9, it is observed that when the $L_{pumping}$ distance is 6m, there is a sharp decline as the distance from working face increases in dust concentration trends, with the highest average concentration exceeding 900mg/m^3. Conversely, for $L_{pumping}$ distances ranging from 1 to 5m, the dust distribution tends to stabilize, effectively controlling the DPM-C within the range of 300mg/m^3. Specifically, at 1m $L_{pumping}$, the DPM-C of dust reaches 310mg/m^3, while at 3m $L_{pumping}$, the dust removal efficiency is optimal, reducing the DPM-C to 250mg/m^3. This reduction is beneficial for the overall well-being, health, and safety of construction workers. Further comprehensive analysis of the simulation results and data comparison reveals that with a fixed pressure outlet location, if the distance between the air pumping port is small, a significant amount of dust remains unsucked and diffuses throughout the entire tunnel area. Conversely, when the distance between the air pumping duct is large, a substantial portion of dust cannot be effectively removed and is instead diffused due to the wind flow impact, leading to higher dust concentrations near the working face. Therefore, it is concluded that the optimal parameter for the air pumping port location and distance from the working face is $L_{pumping}$ at 3m. By implementing this parameter in the primary roadheader construction area, the DPM-C can be effectively controlled within the range of 250mg/m^3, thereby enhancing the overall construction operation environment within the boring tunnel.

Effect of pumping air volume on velocity distribution and dust distribution

Selecting the optimal pumping air volume can lower the fan's energy consumption, as long as the tunnel's flow requirements are met. To study the effect of pumping air volume on dust concentration, the simulation involved setting fixed parameters for $L_{pumping}$ at 3m and $L_{pressure}$ at 20m, while fixing the pressure air volume at 600 m^3/min. The pumping air volume was adjusted to achieve a pumping ratio(r) of less than 1. Subsequently, different pumping ratio (r) were selected at 0.4, 0.5, 0.6, 0.7, 0.8, and 0.9 for numerical simulation. This corresponded to pumping air volumes of 240 m^3/min, 300 m^3/min, 360 m^3/min, 420 m^3/min, 480 m^3/min, and 540 m^3/min. The simulation results, depicted in Figure 10and 11.

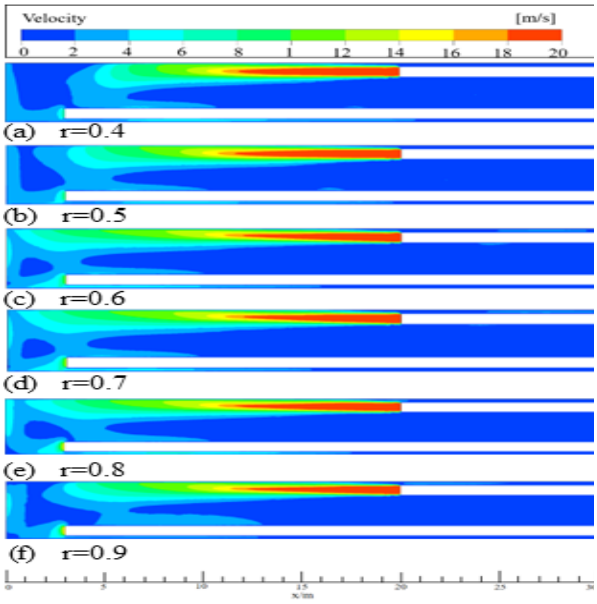

Fig. 10 – Velocity distribution of flow field at 1.5m above ground level for different pumping ratio and less than 1: (a)r=0.4; (b)r=0.5; (c)r=0.6; (d)r=0.7; (e)r=0.8; (f)r=0.9

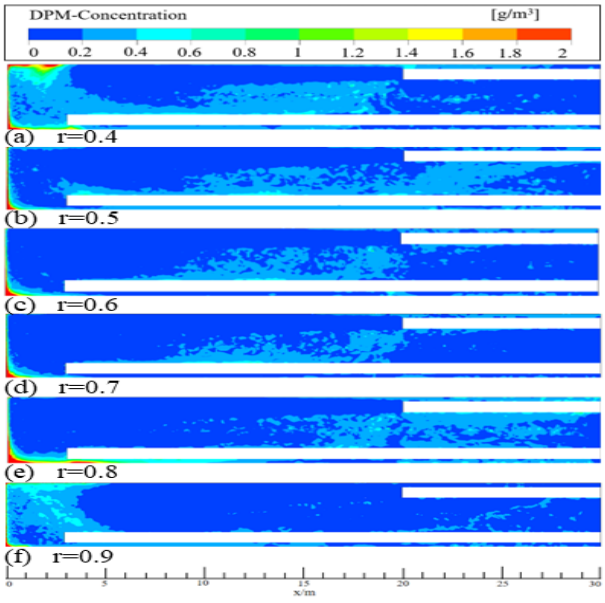

Fig. 11 – Distribution of dust concentration at 1.5m above ground level for different pumping ratio and less than 1: (a)r=0.4; (b)r=0.5; (c)r=0.6; (d)r=0.7; (e)r=0.8; (f)r=0

Upon comparison of Figure 10 and 11, it is evident that a decrease in the value of r, signifying a reduction in the pumping air volume, leads to the continuous dispersion of dust throughout the tunnel due to the influence of the wind flow. When the pumping air volume is significantly lower than the pressing air volume, the pressing air outlet generates wind that disperses dust within the tunnel. For r values of 0.4 and 0.5, depicted in Figure 10(a), (b) and Figure 11(a), (b), the insufficient pumping air volume fails to capture dust emitted from the working face during construction, resulting in low wind flow rates at the duct overlap. Consequently, unsucked dust drifts towards the tunnel opening, causing dust accumulation at the duct overlap and throughout the tunnel area, including the corners adjacent to the working face. In contrast, for r values of 0.6, 0.7, and 0.8 shown in Figure 10 (c), (d), (e) and Figure 11(c), (d), (e), the pumping air volume adequately matches the dust volume produced, facilitating effective dust removal via the pumping duct. When r equals 0.6, 0.7, and 0.8, the dust distribution in the tunnel remains similar, with lower dust concentrations diffusing up to 15-20m from the working face. and up to 30m for r equals 0.8. Additionally, limited diffusion of lower dust concentrations occurs along the tunnel wall due to pressure-induced airflow into the ducts. For r equals 0.9, as depicted in Figure 10(f) and Figure 11(f), the pumping and pressing air volumes are approximately equivalent, resulting in reduced airflow velocity around the pumping duct. Consequently, a substantial accumulation of dust occurs at the working face, leading to high dust concentration and decreased dust suction efficiency by the pumping duct.

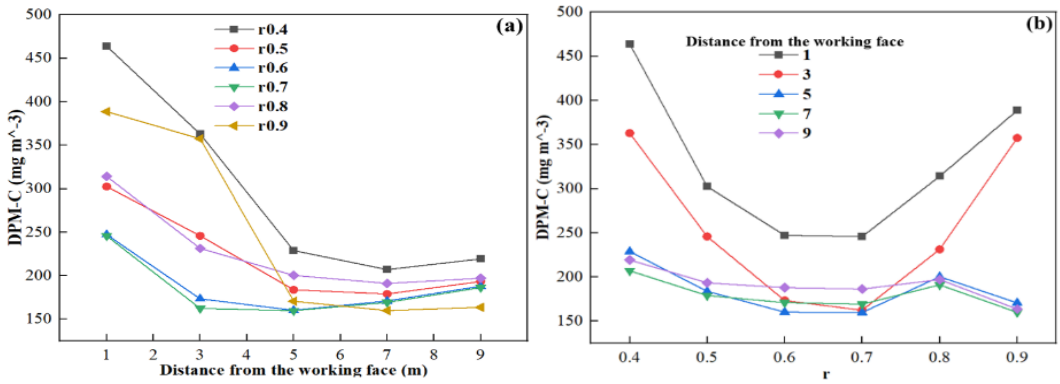

Fig. 12– Comparison of along-track distribution of dust concentration for different pumping ratio: (a) pumping ratio less than 1; (b) different distances from the working face.

When examining Figure 12(a), it is evident that when r falls below 1, the overall dust concentration demonstrates a declining pattern as the distance from the working face increases within the range of 0m to 5m (0<X<5m) from the working face. Progressively, the concentration then tends to stabilize between the distances of 5m to 10m (5<X<10m) from the working face. Figure 12(b) illustrates that in the primary construction operational zone, the highest average dust concentration surpasses 350mg/m^3 for r values of 0.4 and 0.9. Similarly, for r values of 0.5 and 0.8, the highest average concentration of dust exceeds 300mg/m^3. Conversely, for r values of 0.6 and 0.7, the average dust concentration remains below 250mg/m^3. Furthermore, the average concentration of dust can be diminished notably when r equals 0.7, as depicted in Figure 12 (b). Remarkably, the reduction in average dust concentration is more pronounced at r equal to 0.7, as clearly illustrated in the figure.

Base on the comprehensive analysis of the simulation results and data comparison, it is inferred that when the pumping air volume is less than the pressing air volume (r < 1), the optimal r equals 0.7. Maintaining this pumping ratio facilitates effective coordination between the pressure and pumping airflows, thereby enhancing the performance of the ventilation system for tunnel ventilation and dust removal.

Effect of pressure air volume on velocity distribution and dust distribution

To study the effect of pressure air volume on dust concentration, fixed $L_{pumping}$ was maintained for 3 m and $L_{pressure}$ for 20 m. Fixed pumping air volume at 600 m^3/min. The pressure air volume was adjusted to achieve a pumping ratio(r) greater than 1. Following this, numerical simulations were conducted with different pumping ratio (r) of 1.1, 1.2, 1.5, 1.6, 1.8, and 2. As a result, the simulated pumping air volumes were 660 m^3/min, 720 m^3/min, 900 m^3/min, 960 m^3/min, 1080 m^3/min, and 1200 m^3/min respectively. The simulation outcomes, depicted in Figure 13 and 14.

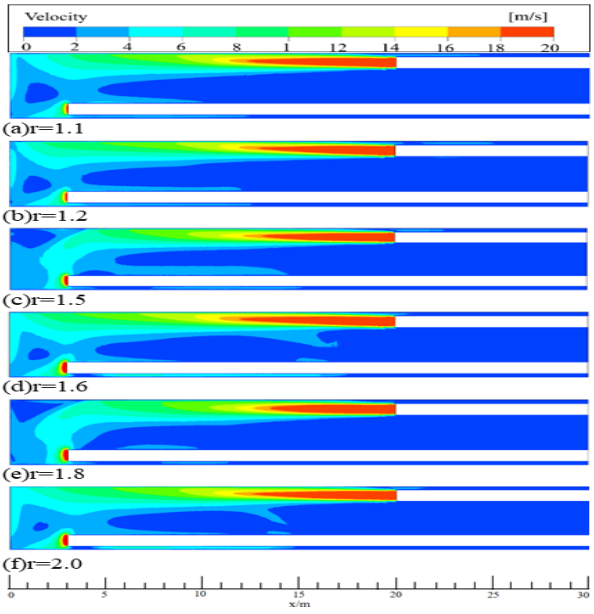

Fig. 13 – Velocity distribution of the flow field at different pumping ratio and greater than 1: (a) r=1.1; (b) r=1.2;(c) r=1.5;(d) r=1.6;(e) r=1.8;(f) r=2.0

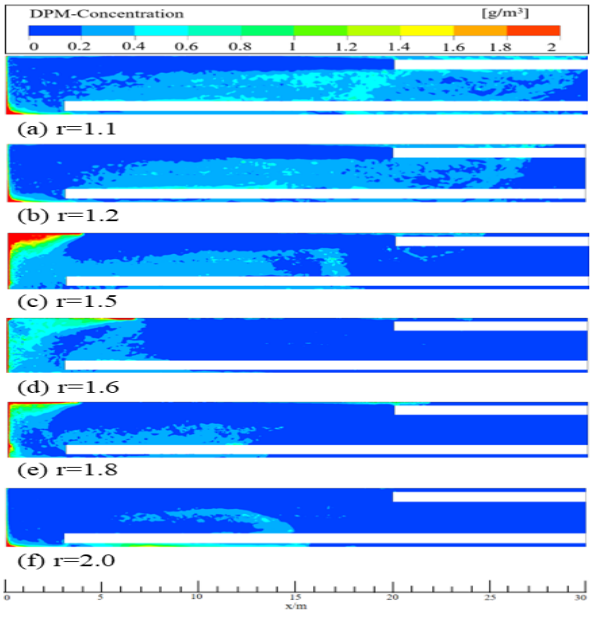

Fig. 14 – Distribution of dust concentration at different pumping ratio greater than 1: (a) r=1.1; (b) r=1.2;(c) r=1.5;(d) r=1.6;(e) r=1.8;(f) r=2.0

Upon comparing Figure 13 and 14, it is evident that with an increase in r, signifying an increase in the pumping air volume, the diffusion distance of the dust decreases gradually due to the influence of wind flow. When r values are at 1.1 and 1.2, illustrated in Figure 13(a) and (b), and Figure 14(a) and (b), the pumping air volume slightly surpasses the pressing air volume. There is a smaller discrepancy between the air volumes in the two ducts and a noticeable impact of the pumping air on the dust concentration around the working face, leading to lower dust concentration levels. Despite this, the pumping air fails to establish an effective flow field interaction with the pressing air, causing ineffective dust suction at the outlet. Consequently, the dust is inadequately removed, leading to its widespread distribution throughout the tunnel space and a diminished ventilation effect. As r increases to 1.5, 1.6, and 1.8, depicted in Figure 13(c), (d), and (e), and Figure 14(c), (d), and (e), the dust diffusion distance diminishes gradually due to the escalating difference between the pumping and pressing air volumes. The enhanced suction effect of the pumping propels the pressing air flow and the tunnel air towards the working face. This leads to the accumulation of dust primarily in the vicinity of the working face, resulting in higher dust concentration levels, confined within a range of approximately 5m from the working face. As r equals 2, showcased in Figure 13(f) and 14(f), the pumping air volume markedly surpasses the pressing air volume. The potent suction effect of the pumping successfully removes most of the dust, transferring it to the pumping air duct. Simultaneously, the pressing air conveys the remaining low-concentration dust towards the pumping air outlet, with some minor amounts spreading towards the pumping air duct's side and the tunnel wall within a range of 10-15m from the working face. Consequently, the expansion distance and

coverage area are relatively few, enhancing the efficiency of dust removal in this scenario.

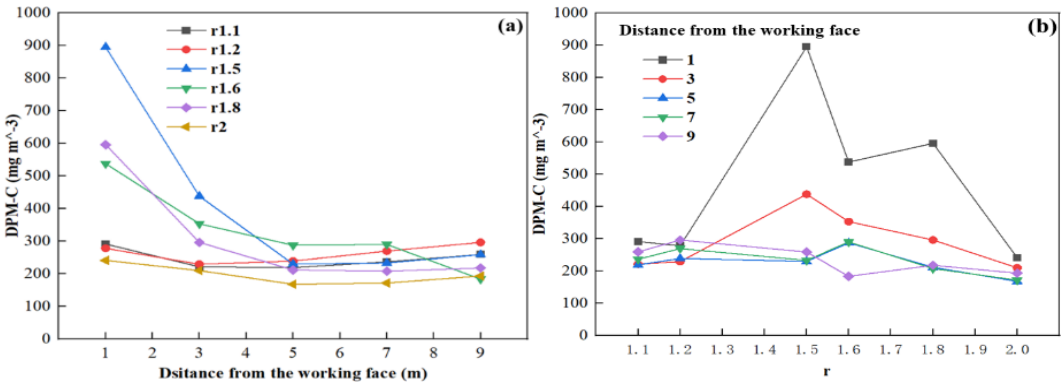

Fig. 15 – Comparison of along-track distribution of dust concentration for different pumping ratio greater than 1: (a) pumping ratio greater than 1; (b) different distances from the working face.

As can be seen from Figure 15, in the main construction work area, the dust concentration within 5m (0<X<5m) from the working face exhibits a sharp decline as the distance from the working face increases when r values are 1.5, 1.6, and 1.8, followed by a tendency to stabilize. However, despite this trend, the highest DPM-C of dust exceeds 530 mg/m^3, indicating that the dust removal effectiveness is not optimal. On the other hand, for r values of 1.1, 1.2, and 2, the dust concentration remains relatively stable, hovering around 300 mg/m^3 within 10m (0<X<10m) from the working face. Notably, when r equals 2, the DPM-C of dust can be effectively maintained within the range of 250 mg/m^3.

It is concluded, based on a comprehensive analysis of the simulation results and data comparisons, that when the pumping air volume exceeds the pressing air volume (r > 1), the optimal parameter for r is 2. However, under these circumstances, the pumping air duct also draws in fresh air, leading to an inadequate supply of fresh air in the tunnel, which necessitates a higher level of performance for the dust fan. Furthermore, fans with large air volumes typically consume more energy, resulting in higher production costs for manufacturers and potential wastage. As a result, in practical working conditions, a higher pumping ratio is generally not recommended.

3.5 Simulation verification

Based on several sets of simulation results, the optimal values of the tunnel ventilation system layout parameters are obtained: the $L_{pumping}$ is 3 m, the $L_{pressure}$ is 20 m, and the pumping ratio (r) is 0.7. Further numerical simulations are carried out to verify the accuracy of the ventilation layout parameters by simulating the ventilation and dust removal effects of the tunnel ventilation system under these layout parameters. The simulation results are shown in Fig.16.

As depicted in Figure 16, the majority of the dust is effectively removed by the suction duct or carried away by the tunnel wind flow, resulting in optimal ventilation and dust removal efficiency. It is evident that only a minor fraction of dust disperses to the tunnel between the distances of 12-30m from the working face, exhibiting low concentration levels. Conversely, in the crevices and corners of the working face adjacent to the duct and the tunnel wall, there is a small area of significant dust accumulation with high concentration levels.

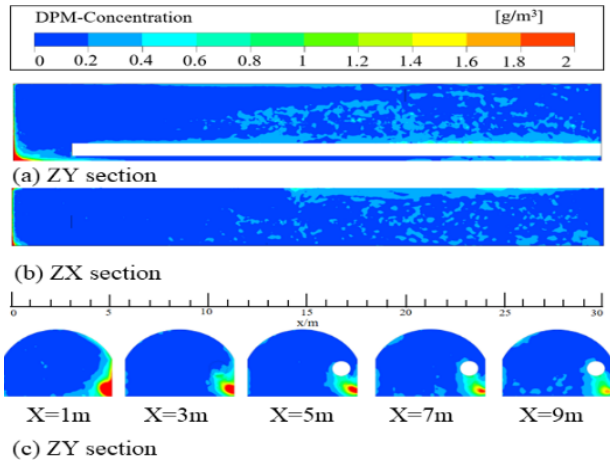

Fig. 16 – Distribution of dust concentration in different cross sections after optimal design: (a) ZY section; (b) ZX section; (c) ZY section

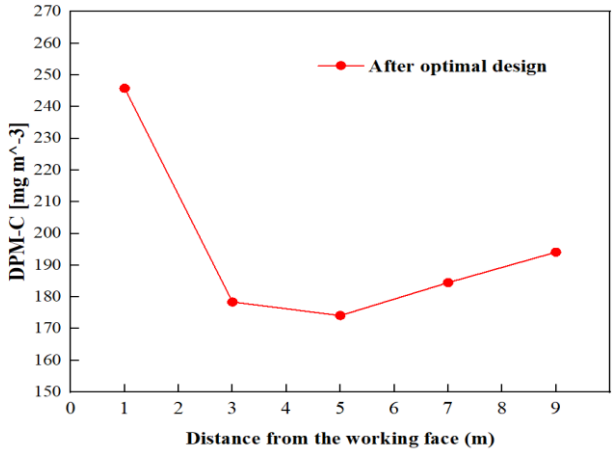

Fig. 17 – Distribution of dust concentration along the course of the optimal design

Figure 17 illustrates the effective control of dust mass concentration in the main construction area of the tunnel, remaining within the range of 250mg/m^3. Specifically, the highest DPM-C of 245.8mg/m^3 is observed within 3m (0<X<3m) from the tunnel's face, while the mass concentration remains below 200mg/m^3 within 3-10m (3<X<10m) from the tunnel's face. This controlled environment is conducive for construction workers to carry out their tasks efficiently. Therefore, the data accuracy and credibility of the optimal arrangement parameter can be substantiated.

CONCLUSION

The optimal values for the tunnel ventilation system parameters were found to be 20m for $L_{pressure}$, 3m for $L_{pumping}$, and a pumping ratio of 0.7, as revealed by the results. Specifically, under these parameters, the dust particulate matter concentration (DPM-C) can be successfully controlled within the range of 250mg/m3. Therefore, the numerical simulation outcomes not only provide a theoretical foundation but also offer guidance for the appropriate arrangement of air ducts and management of dust concentration in the tunnel ventilation system when similar operating conditions are encountered.

In this paper, only the condition of ventilation duct arrangement has been considered, and

whether the duct length should be proportionally increased for longer tunnels as well as adjusting the angle of the air duct and the working face still needs to be explored in the future.

ACKONWLEDGEMENT

This research is supported by the National Natural Science Foundation of China (Granted No. 52005179), the Scientific Research Project of Hunan Education Department (Granted No. 20C1153), the Natural Science Foundation of Hunan Province (Granted No.2020JJ5365).

REFERENCE

[1] Zhou W, Nie W, Liu X, et al. Optimization of dust removal performance of ventilation system in tunnel constructed using shield tunneling machine[J]. Building and Environment. 2020, 173: 106745.

[2] Hua Y, Nie W, Liu Q, et al. The development and application of a novel multi-radial-vortex-based ventilation system for dust removal in a fully mechanized tunnelling face[J]. Tunnelling and Underground Space Technology. 2020, 98: 103253.

[3] Menéndez J, Fernández-Oro J M, Merlé N, et al. Auxiliary ventilation systems in mining and tunnelling: Air leakage prediction and system design to optimize the energy efficiency and operation costs[J]. Tunnelling and Underground Space Technology. 2023, 140: 105298.

[4] Ates U, Copur H. Investigation of parameters affecting vibration patterns generated during excavation by EPB tbms[J]. Tunnelling and Underground Space Technology. 2023, 138: 105185.

[5] Lehmann G, Käsling H, Hoch S, et al. Analysis and prediction of small-diameter TBM performance in hard rock conditions[J]. Tunnelling and Underground Space Technology. 2024, 143: 105442.

[6] Li J, Guo D, Chen Z, et al. Transfer learning for collapse warning in TBM tunneling using databases in China[J]. Computers and Geotechnics. 2024, 166: 105968.

[7] Ni S, Chao B T, Soo S L. Particle diffusivity in fully developed, turbulent, horizontal pipe flow of dilute air—solid suspensions[J]. International Journal of Multiphase Flow. 1990, 16(1): 43-56.

[8] Hargreaves D M, Lowndes I S. The computational modeling of the ventilation flows within a rapid development drivage[J]. Tunnelling and Underground Space Technology. 2007, 22(2): 150-160.

[9] Parra M T, Villafruela J M, Castro F, et al. Numerical and experimental analysis of different ventilation systems in deep mines[J]. Building and Environment. 2006, 41(2): 87-93.

[10] Wang H, Cheng W, Sa Z, et al. Experimental study of the effects of air volume ratios on the air curtain dust cleaning in fully mechanized working face[J]. Journal of Cleaner Production. 2021, 293: 126109.

[11] Lai A C K. Modeling indoor coarse particle deposition onto smooth and rough vertical surfaces[J]. Atmospheric Environment. 2005, 39(21): 3823-3830.

[12] Hussein T, Hruška A, Dohányosová P, et al. Deposition rates on smooth surfaces and coagulation of aerosol particles inside a test chamber[J]. Atmospheric Environment. 2009, 43(4): 905-914.

[13] Klemens R, Kosinski P, Wolanski P, et al. Numerical study of dust lifting in a channel with vertical obstacles[J]. Journal of loss prevention in the process industries. 2001, 14(6): 469-473.

[14] Sa Z, Li F, Qin B, et al. Numerical simulation study of dust concentration distribution regularity in cavern stope[J]. Safety Science. 2012, 50(4): 857-860.

[15] Ashrafi K, Shafie-Pour M, Kalhor M, et al. Numerical Simulation of Air Pollutant Distribution in Urban

Tunnels[J]. Environmental Modeling & Assessment. 2012, 17(5): 555-564.

[16] Toraño J, Torno S, Menéndez M, et al. Auxiliary ventilation in mining roadways driven with roadheaders: Validated CFD modelling of dust behaviour[J]. Tunnelling and Underground Space Technology. 2011, 26(1): 201-210.

[17] Lee S, Lee S, Lee J. CFD analysis on ventilation characteristics of jet fan with different pitch angle[J]. KSCE Journal of Civil Engineering. 2014, 18(3): 812-818.

[18] Liu Q, Nie W, Hua Y, et al. A study on the dust control effect of the dust extraction system in TBM construction tunnels based on CFD computer simulation technology[J]. Advanced Powder Technology. 2019, 30(10): 2059-2075.

[19] Xie Z, Ruan C, Zhao Z, et al. Effect of ventilation parameters on dust pollution characteristic of drilling operation in a metro tunnel[J]. Tunnelling and Underground Space Technology. 2023, 132: 104867.

[20] Yang X, Yu H, Wang Y, et al. Investigation of dust pollution control rules in tunnel excavation based on modularized airflow diverging system[J]. Building and Environment. 2022, 221: 109356.

[21] Von Glehn F H, Bluhm S J. Practical aspects of the ventilation of high-speed developing tunnels in hot working environments[J]. Tunnelling and underground space technology. 2000, 15(4): 471-475.

[22] Xia Y, Yang D, Hu C, et al. Numerical simulation of ventilation and dust suppression system for open-type TBM tunneling work area[J]. Tunnelling and Underground Space Technology. 2016, 56: 70-78.

[23] Liu X, Nie W, Zhou W, et al. The optimization of a dust suppression and clean production scheme in a TBM-constructed tunnel based on an orthogonal experiment[J]. Process Safety and Environmental Protection. 2020, 136: 353-370.

[24] Li S, Jin H, Hu S, et al. Experimental investigation and field application of pulse-jet cartridge filter in TBM tunneling construction of Qingdao Metro Line 8 subsea tunnel[J]. Tunnelling and Underground Space Technology. 2021, 108: 103690.

[25] Eftekharian E, Dastan A, Abouali O, et al. A numerical investigation into the performance of two types of jet fans in ventilation of an urban tunnel under traffic jam condition[J]. Tunnelling and Underground Space Technology. 2014, 44: 56-67.

[26] Wang J, Levy E K. Particle motions and distributions in turbulent boundary layer of air–particle flow past a vertical flat plate[J]. Experimental Thermal and Fluid Science. 2003, 27(8): 845-853.

[27] Chang P, Xu G, Huang J. Numerical study on DPM dispersion and distribution in an underground development face based on dynamic mesh[J]. International Journal of Mining Science and Technology. 2020, 30(4): 471-475.

[28] van Wachem B G M, Almstedt A E. Methods for multiphase computational fluid dynamics[J]. Chemical Engineering Journal. 2003, 96(1-3): 81-98.

[29] Cai P, Nie W, Chen D, et al. Effect of air flowrate on pollutant dispersion pattern of coal dust particles at fully mechanized mining face based on numerical simulation[J]. Fuel. 2019, 239: 623-635.

[30] Wan W, Li X, An N. Study on the reasonable position of the wind pipe of the long-pressure-short-drawing ventilation system of the comprehensive excavation working face [J]. Coal Technology. 2019, 38(04): 123-125. (in Chinese)